AAV9 delivering a modified human Mullerian inhibiting substance as a gene therapy in patient-derived xenografts of ovarian cancer

David Pépin[a,1], Amanda Sosulski[a,1], Lihua Zhang[a], Dan Wang[b], Vinod Vathipadiekal[c], Katherine Hendren[a], Caroline M. Coletti[a], Aaron Yu[a], Cesar M. Castro[c], Michael J. Birrer[c], Guangping Gao[b], and Patricia K. Donahoe[a,2]

[a]Pediatric Surgical Research Laboratories, Massachusetts General Hospital, Department of Surgery, Harvard Medical School, Boston, MA 02114; [b]Gene Therapy Center, University of Massachusetts Medical School, Worcester, MA 01655; and [c]Gynecological Oncology, Massachusetts General Hospital, Department of Medicine, Harvard Medical School, Boston, MA 02114

Contributed by Patricia K. Donahoe, June 21, 2015 (sent for review May 1, 2015; reviewed by Richard N. Freiman, Charles N. Landen Jr, and Anil K. Sood)

To improve ovarian cancer patient survival, effective treatments addressing chemoresistant recurrences are particularly needed. Mullerian inhibiting substance (MIS) has been shown to inhibit the growth of a stem-like population of ovarian cancer cells. We have recently engineered peptide modifications to human MIS [albumin leader Q425R MIS (LRMIS)] that increase production and potency in vitro and in vivo. To test this novel therapeutic peptide, serous malignant ascites from highly resistant recurrent ovarian cancer patients were isolated and amplified to create low-passage primary cell lines. Purified recombinant LRMIS protein successfully inhibited the growth of cancer spheroids in vitro in a panel of primary cell lines in four of six patients tested. Adeno-associated virus (AAV) -delivered gene therapy has undergone a clinical resurgence with a good safety profile and sustained gene expression. Therefore, AAV9 was used as a single i.p. injection to deliver LRMIS to test its efficacy in inhibiting growth of palpable tumors in patient-derived ovarian cancer xenografts from ascites (PDXa). AAV9-LRMIS monotherapy resulted in elevated and sustained blood concentrations of MIS, which significantly inhibited the growth of three of five lethal chemoresistant serous adenocarcinoma PDXa models without signs of measurable or overt toxicity. Finally, we tested the frequency of MIS type II receptor expression in a tissue microarray of serous ovarian tumors by immunohistochemistry and found that 88% of patients bear tumors that express the receptor. Taken together, these preclinical data suggest that AAV9-LRMIS provides a potentially well-tolerated and effective treatment strategy poised for testing in patients with chemoresistant serous ovarian cancer.

MIS | anti-Mullerian hormone | ovarian cancer | PDX | AAV9

Ovarian cancer is an enigmatic disease with 70% recurrence, and it is almost invariably fatal, even after complete response to chemotherapy and debulking i.p. surgery. Newer agents, such as angiogenesis inhibitors (1, 2) or ADP-ribose polymerase inhibitors (3), have only provided short-term improvement to survival outcomes. A dire need exists to develop novel therapeutic strategies addressing those highly chemoresistant recurrences that drive mortality. Epithelial ovarian cancers have long been known as "Mullerian" tumors, because histopathology of serous cystadenocarcinoma, endometrioid, and mucinous carcinomas recapitulates the embryonic Mullerian duct, the anlagen of the fallopian tube, uterus, cervix, and upper vagina (4). Hence, we turned to Mullerian inhibiting substance (MIS; also known as anti-Mullerian hormone), an evolutionarily conserved endogenous hormone of fetal and adult gonads (5), as a therapeutic against Mullerian-derived ovarian cancer. Recombinant human MIS (rhMIS) produced using a genomic clone (6) and purified from CHO serum-free media (7, 8) caused regression of fetal Mullerian ducts ex vivo and inhibited mouse ovarian cancer cell lines generated by *Misr2-Cre* directing T antigen in vitro and in vivo (9, 10). Similar effects were evident in established human ovarian cancer cell lines in vitro (11) and in vivo (12, 13). We also discovered that rhMIS targets a stem/progenitor cell population present in transgenic (14) and established human ovarian cancer cell lines (11, 15). However, rhMIS potency was limited in this heterogeneous product by low primary cleavage required for bioactivity. To address these concerns, we engineered new modified cDNA constructs that provide an MIS protein with increased primary cleavage, reduced secondary cleavage, and increased potency and homogeneity by altering the cleavage site and the leader peptide sequence (16).

The new engineered MIS analog, albumin leader Q425R MIS (LRMIS), was placed in a recombinant adeno-associated virus serotype 9 (rAAV9) vector that, when delivered as a single injection, produces high and sustained serum levels of transgene. rAAV is now an accepted gene transfer platform technology because of its wide range of tissue tropisms, low immunogenicity, highly efficient and sustained gene transduction, and clinically proven track record of safety evident in the treatments of Leber's congenital amaurosis, hemophilia B, Parkinson's disease, and other disorders (17). The ability to sustain therapeutic levels of MIS with a single injection provides a unique opportunity to screen a large cohort of patient-derived ovarian cancer xenografts from ascites (PDXa) models and develop predictive readouts of response. Patient xenografts have been shown to match the architecture and histotype of the patient's

Significance

To improve ovarian cancer patient survival, effective treatments addressing chemoresistant recurrences are particularly needed. Mullerian inhibiting substance (MIS) has been shown to inhibit the growth of a stem-like population of ovarian cancer cells. To test this protein therapeutic, malignant ascites from patients with highly resistant recurrent ovarian cancer were used to create patient-derived ovarian cancer xenografts. Mice bearing tumors were treated with adeno-associated virus serotype 9 gene therapy delivering MIS, which inhibited three of five models without signs of toxicity. Finally, we found that 88% of serous tumors express MIS type II receptor by immunohistochemistry. These preclinical data suggest that gene therapy with MIS provides a potentially well-tolerated and effective treatment strategy for chemoresistant serous ovarian cancer.

Author contributions: D.P., A.S., C.M. Castro, G.G., and P.K.D. designed research; D.P., A.S., L.Z., K.H., and A.Y. performed research; D.W., V.V., M.J.B., and G.G. contributed new reagents/analytic tools; D.P., A.S., and P.K.D. analyzed data; and D.P., C.M. Coletti, and P.K.D. wrote the paper.

Reviewers: R.N.F., Brown University; C.N.L., University of Virginia; and A.K.S., University of Texas MD Anderson Cancer Center.

The authors declare no conflict of interest.

[1]D.P. and A.S. contributed equally to this work.

[2]To whom correspondence should be addressed. Email: pdonahoe@partners.org.

This article contains supporting information online at www.pnas.org/lookup/suppl/doi:10.1073/pnas.1510604112/-/DCSupplemental.

www.pnas.org/cgi/doi/10.1073/pnas.1510604112

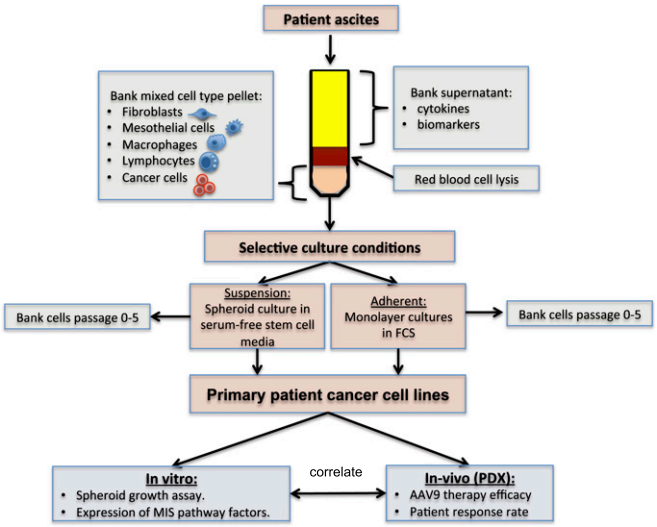

Fig. 1. Primary cancer cell lines derived from ovarian cancer ascites samples. Fresh ascites samples are centrifuged, and the cell pellet and supernatant are reserved. The cell pellet is treated with RBC lysis buffer and introduced into culture in two conditions: suspension or adherent. In suspension culture, only the nonadherent cells are passaged in serum-free spheroid media. In adherent cultures, cells are grown and maintained at confluency in serum-containing media until tight epithelial colonies displace contact-inhibited normal cells. The culture is then partially trypsinized, so that only tightly adherent cancer cells remain. Low-passage cell cultures can then be used for in vitro and in vivo experiments or stored in liquid nitrogen for future use.

primary tumor, conserve the same gene expression profile and genetic aberrations (18), maintain cellular heterogeneity, and mirror the response to treatment observed in the patient (19), making them ideally suited for therapeutic testing.

These experiments show the feasibility of using adeno-associated virus serotype 9 (AAV9) vectors to screen PDXa responsiveness in vivo in a large number of patients and underscore the timeliness of MIS clinical development. Gene therapy delivery of LRMIS with AAV9 viral vectors portends single-injection adjuvant treatment for ovarian cancer with potential for therapeutic inroads in the chemoresistant setting.

Results

Primary Ovarian Cancer Cell Lines Derived from Patient Ascites Express MIS Type II Receptor, and a Subset Is Tumorigenic in Mice. The cellular fractions from 41 ascites samples were collected, processed, and placed in culture conditions to ensure that the cancer cells were enriched selectively. Cancer cells were grown for a limited number of passages (three to five) either as monolayer cultures in media-containing serum or in suspension in spheroid media (Fig. 1 and Table 1); 39% of these ascites samples generated primary cancer cell lines, including 14 serous ovarian cancer lines [patient D (ptD), ptH, PKD1, PKD2, ptU, ptW, ptY, ptAB, ptAF, ptAI, ptAK, ptAM, ptAO, and ptAL], one endometrioid line (ptAP), and one mucinous cell line (ptG) (Table 1). Although most patient cancer cells grew as both monolayers and spheroids (ptH, ptG, ptU, ptW, ptAB, ptAF, ptAK, ptAO, ptAP, and ptAL), some cell lines were only able to grow in adherent conditions (ptD, PKD1, PKD2, ptY, and ptAI), whereas others only grew in suspension (ptAM-sph) (Table 1 and Fig. S1). All primary cell lines tested expressed MIS type II receptor (MISRII) protein by Western blot, regardless of culture condition (Fig. 2*A*); MISRII protein levels were found to be generally equal or slightly lower in spheroid suspension cultures than in adherent monolayer cultures of cells from the same patient (Fig. S2*A*). Tumorigenicity of the low-passage primary cell lines was tested; eight (50%) formed tumors after engraftment of 5–10 M cells s.c. in the flanks of pairs of NOD/SCID/IL2Rg (NSG) mice, and all recapitulated patients' primary tumor histology. Tumor growth rates were variable, with the time to reach 100 mm^3 ranging from 7 (ptD) to 150 d (ptH). Interestingly, for some of these patient cells, such as ptAB, the spheroid cultures were much more tumorigenic than the adherent monolayers (Fig. S2 *B* and *C*). Five cell lines were chosen to carry out the in vivo experiments as PDXas (ptD, ptAB, ptAM, ptW, and ptH), because they reliably formed tumors in mice with 100% engraftment rates, and all were of serous histology. This panel of five PDXa formed tumors that expressed MISRII as evidenced by immunohistochemical staining (Fig. 2*B*). Expression of MISRII was homogenous in the epithelial compartment of the tumors and uniformly excluded from the stromal compartment; staining was both cytoplasmic and membranous.

Primary Cancer Spheroids Were Enriched in Progenitor Markers, Expressed MIS Signaling Pathway Genes, and Were Inhibited by Purified Recombinant Flag-Tagged LRMIS Protein. To verify that primary spheroid growth conditions allow the retention of the cancer stem cell phenotype, we compared expression levels of pluripotency markers (OCT4, LIN28, SOX2, and KLF4) in matched cell lines cultured in both adherent and suspension culture conditions by quantitative PCR (qPCR) and found enhanced expression of at least one of the markers (normalized to adherent condition) in spheroids, suggesting heterogeneity in marker expression among the primary cell lines (Fig. 3*A*). To test the responsiveness of the primary patient cell lines to MIS therapy, a panel of cells capable of growth in nonadherent condition (ptAB-sph, ptAF-sph, ptAM-sph, ptAO-sph, ptAP-sph, and ptW-sph) was tested in a spheroid growth assay in serum-free spheroid media. Small nascent spheroids were collected and plated individually in single wells of a round-bottomed 96-well plate. Then, they were treated with either 5 μg/mL Flag-tagged LRMIS (LRFMIS) or control (equal volume mock eluate) or left untreated, and spheroid volume was measured at least two times per week for 12–25 d. Treatment with LRFMIS significantly inhibited spheroid growth in four of six cell lines: ptAM-sph, ptAO-sph, ptAP-sph, and ptW-sph (Fig. 3*B*).

To confirm that the primary patient cell lines tested have the necessary signaling machinery for the canonical MIS pathway, expression levels were measured by qPCR of the type II receptor (MISRII), type I receptors (ALK2, ALK3, and ALK6), activating receptor SMADs (SMAD1, SMAD5, and SMAD8/9), co-SMADs (SMAD4), inhibitory SMADs (SMAD6 and SMAD7), and the SMURF ubiquitin ligases (SMURF1 and SMURF2) (Fig. 3*C*). We find that all of the components of the MIS signaling pathway are ubiquitously expressed, with the exception of the activating R-SMAD8/9 and the inhibitory SMAD6, which were absent in ptAM-sph (a responder) and ptAB-sph (a nonresponder).

AAV9 Delivered i.p. Has Tropism to the Muscles and Results in High Secretion Rates of LRMIS. An AAV9 construct designed to deliver LRMIS by gene therapy includes a ubiquitous CMV enhancer fused with chicken β-actin promoter, a synthetic intron, the LRMIS gene, and a rabbit β-globin poly-A signal (Fig. 4*A*). The human LRMIS transgene differs from the endogenous WT human MIS genes by the substitution of its endogenous leader peptide (L) with that of human serum albumin and the introduction of a Q425R substitution (R) at the cleavage site to enhance proteolytic activation (16). A single i.p. administration of 3E11 viral particles of AAV9-GFP control virus in Nu/Nu mice resulted in GFP expression (60 d later) mainly in muscles of the abdomen (body wall and diaphragm), organs of the peritoneal cavity (omentum, pancreas, and liver) (Fig. 4*B*), and muscle cells distant to the peritoneal cavity (skeletal muscles of the limbs and the heart), suggesting dispersion by the vasculature (20).

Table 1. Ascites-derived primary ovarian cancer cell lines

Cell line		In vitro			Markers		
Name	Histotype	Monolayer	Spheres	In vivo: PDXa	MISRII (cell line)	MISRII (tumor)	Mutations: tumor SNaPshot
ptD	Serous	+++	–	Yes	+	+	BRAF
ptG	Mucinous	+++	++	Yes	+	+	
ptH	Serous	++	++	Yes	+	+	
PKD1	Serous	+++	–	No	+		
PKD2	Serous	++	–	No	+		
ptU	Serous	+	+	No	+		BRCA1
ptW	Serous	++	+++	Yes	+	+	
ptY	Serous	+	–	No	+		
ptAB	Serous	++	+++	Yes	+	+	
ptAF	Serous	++	+++	Yes	+		
ptAI	Serous	++	–	No	+		
ptAK	Serous	+	+	No	+		
ptAM	Serous	–	+++	Yes	+	+	
ptAO	Serous	+	+++	No	+		
ptAP	Endometrioid	+	+++	Yes	+	+	KRAS
ptAL	Serous	++	++	No	+		

Other peritoneal organs (kidney, spleen, and gut) as well as organs of the nervous system (brain, eyes, and spinal cord) were not found to express GFP. No fluorescence was detected in any of the organs examined from animals treated with AAV9-LRMIS. The infection did not cause any overt toxicities, changes in behavior, or adverse responses in the mice, and serum levels of common blood toxicity markers, such as cardiac creatine kinase (AAV-LRMIS, 649.5 IU/L; and AAV-GFP, 771.3 IU/L), liver transaminase ALT (AAV-LRMIS, 39.2 IU/L; and AAV-GFP, 32.6 IU/L), AST (AAV-LRMIS, 123.4 IU/L; and AAV-GFP, 112 IU/L), and pancreatic amylase (AAV-LRMIS, 2,850.6 IU/L; and AAV-GFP, 4,418.6 IU/L), were found to be within the normal range. Injections of escalating doses of AAV9-LRMIS (1E10, 1E11, 3E11, and 1E12) i.p. in Nu/Nu mice produced a dose–response of MIS secretion in the blood as determined by ELISA (Fig. 4*C*). Blood levels of MIS were found to be extremely stable during the 60-d extent of the experiment, and injections of 3E11 particles in C57BL6 mice resulted in continued expression for over 1 y. Expression of cleaved MIS C terminus was confirmed by Western blot analysis of body wall muscle lysates and pancreas lysates (Fig. 4 *D* and *E*).

AAV9-LRMIS Pretreatment Significantly Inhibits the Growth of OVCAR5 Xenografts. The efficacy of AAV9-LRMIS pretreatment in inhibiting tumor growth in vivo was first tested in an OVCAR5 xenograft model. Nu/Nu mice were pretreated with either AAV9-LRMIS ($n = 5$) or AAV9-GFP control ($n = 5$) in two separate experiments: one using a dose of 3E11 (Fig. 5*A*) and one with 1E12 viral particles (Fig. 5*B*). MIS levels in the blood were monitored by ELISA for 3 wk, at which point they were found to plateau (Fig. 5 *A*, *Left*

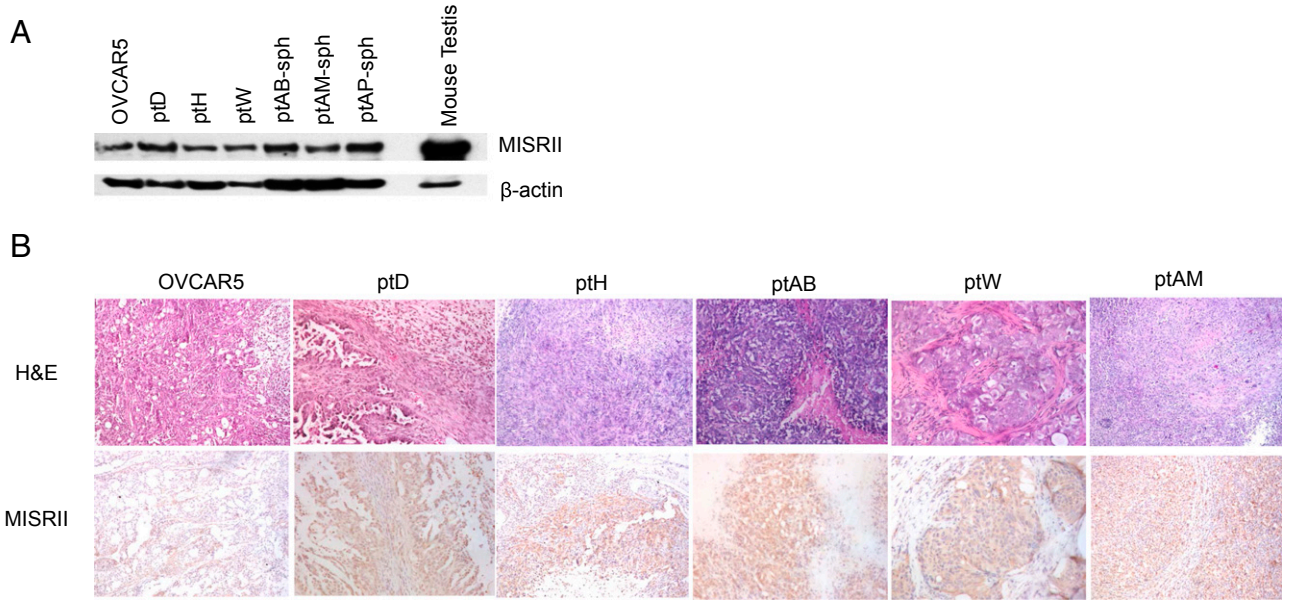

Fig. 2. Primary cancer cell lines express MISRII by Western blot and form tumors positive for MISRII by immunohistochemistry in mice. (*A*) Western blot of protein lysates from a panel of five primary cell lines and OVCAR5 probed for MISRII expression or loading β-actin expression as a control (mouse testis lysate used as a positive control). (*B*) Tumors derived from xenografts of a panel of five primary cell lines and OVCAR5 were fixed and paraffin-embedded. Tumors were stained by H&E or for immunohistochemistry with an antibody against MISRII (H-150) or no primary control, and sections were photographed with 100× magnification.

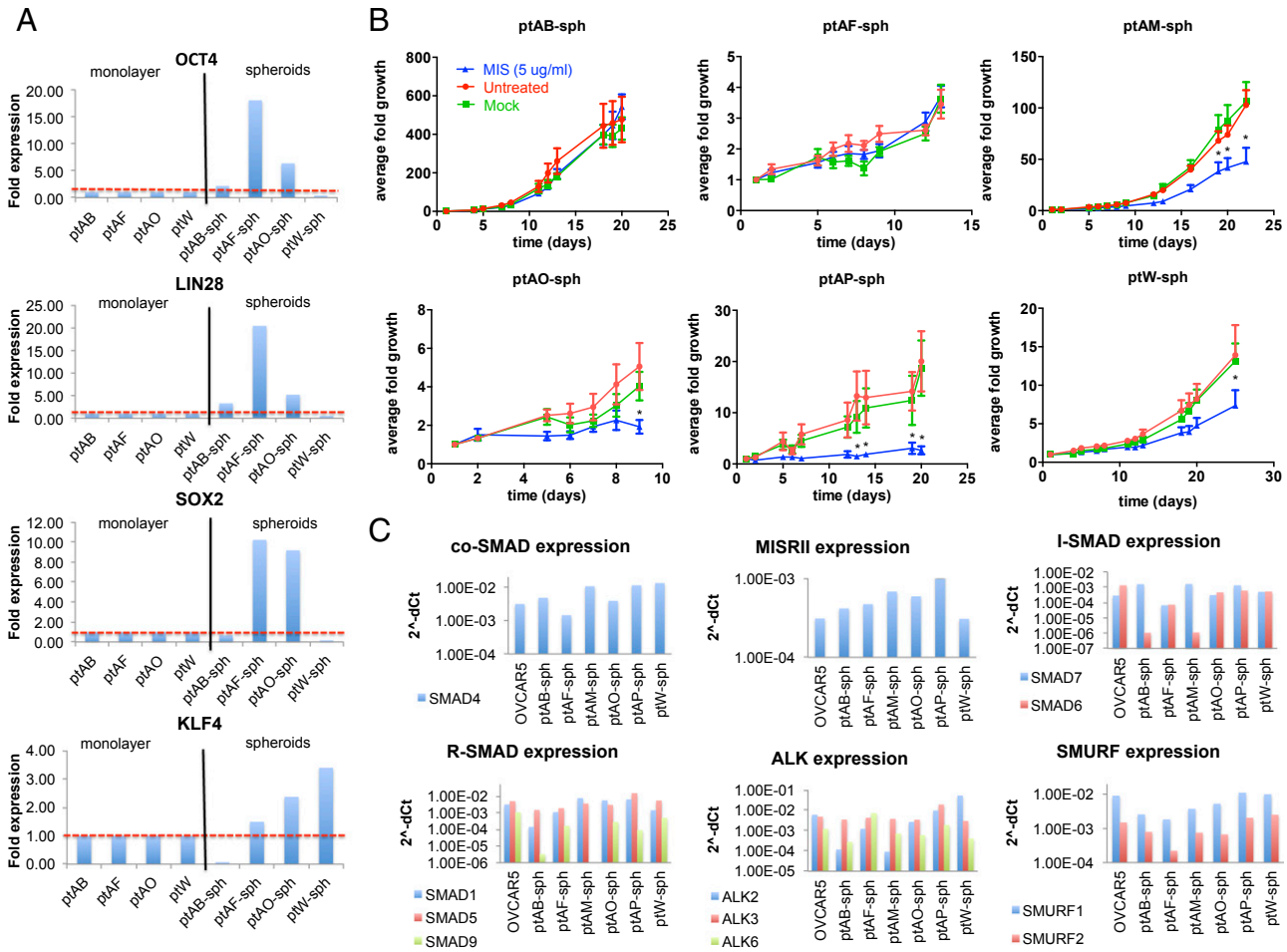

Fig. 3. Patient-derived tumor spheroids express pluripotency markers and components of the MIS signaling pathway and are growth-inhibited by MIS. (*A*) Primary cell lines successfully cultured in paired conditions of adherent monolayers (ptAB, ptAF, ptAO, and ptW) and suspension tumor spheroids (ptAB-sph, ptAF-sph, ptAO-sph, and ptW-sph) were compared by qPCR for relative expression (normalized to monolayer condition) of pluripotency markers (OCT4, LIN28, SOX2, and KLF4). (*B*) Small nascent tumor spheroids were isolated from a panel of six primary ascites cell lines (ptAB-sph, ptAF-sph, ptAM-sph, ptAO-sph, ptAP-sph, and ptW-sph), cultured in suspension, singly plated in a 96-well plate, and then, grown in media with MIS (LRFMIS: 5 μg/mL) or control (mock eluate) or left untreated. Average volume growth of the spheroid represented over time was derived from measurements of length and width using a microscopic ruler: $V = (L \times W \times W)/2$. At least three trials were carried out for each cell line with at least eight spheroids per group, and representative graphs are shown. Data were analyzed by two-way ANOVAs comparing control and MIS treatment. *Posthoc tests of P value significance for each time point ($P < 0.05$). (*C*) Relative expressions of components of the MIS signaling pathways (SMAD4, MISRII, SMAD6, SMAD7, SMAD1, SMAD5, SMAD8/9, ALK2, ALK3, ALK6, SMURF1, and SMURF2) were measured by qPCR in a panel of six primary cell lines (ptAB-sph, ptAF-sph, ptAM-sph, ptAO-sph, ptAP-sph, and ptW-sph), and cycle threshold (Ct) values ($2^{-\Delta Ct}$) are shown.

and *B*, *Left*), and the animals were xenografted s.c. in the flank with 5 M OVCAR5 cells. Growth of the tumors, as determined by weekly caliper measurements, was found to be significantly inhibited by pretreatment with AAV9-LRMIS at both the 3E11 ($P < 0.001$) (Fig. 5*A*, *Right*) and the 1E12 ($P < 0.01$) (Fig. 5*B*, *Right*) doses. Animals were killed after solid tumors reached >20 mm at the largest diameter, became ulcerated, or impaired mobility and the wellbeing of the animal as per animal welfare protocols.

AAV9-LRMIS Posttreatment of Palpable Patient-Derived Xenografts Results in Significant Inhibition of Growth. To test the efficacy of AAV9-LRMIS posttreatment in five PDXa models, primary cell lines (ptW, ptAB-sph, ptH, and ptAM-sph, which form tumors in immunosuppressed NSG mice, or PtD in Nu/Nu mice) were xenografted at 5 M cells per animal s.c. in groups of 10 mice. Tumor volumes were monitored weekly by caliper measurements, and the tumors were allowed to grow until the average tumor volume in those animals reached 100 mm^3. Mice were then treated with AAV9-LRMIS or AAV9-GFP i.p. at 3E11 viral particles per mouse. Tumor volume was monitored by caliper measurements until at least one mouse had a tumor exceeding 20 mm at its largest diameter or other wellness endpoints were met; then, all animals were euthanized, and tumors and blood were harvested. Tumor growth was significantly inhibited by LRMIS treatment in ptW (Fig. 6*A*), ptAB (Fig. 6*B*), and ptH (Fig. 6*C*) but not in ptAM (Fig. 6*D*) or ptD (Fig. 6*E*) PDXas. Interestingly, two of five AAV9-LRMIS–treated mice from the ptW PDXa (Fig. 6*A*) exhibited complete tumor regression within 14 d of treatment, with only microscopic evidence of residual tumor at necropsy in one animal, which was later confirmed by H&E staining. Treated mice were found to have blood levels of 0.5–2 μg/mL MIS at the endpoint, but the blood concentration in complete responders was not significantly different from that in partial responders. Analysis of tumor lysates at the endpoint by Western blot ($n = 3$ for each PDXa) revealed a significant change of P-SMAD1,5,8 in responsive tumors (ptW, ptAB, and ptH) but not in nonresponders (ptD and ptAM). Similarly, cell cycle-modulating proteins P21 and CCND1 displayed trends of alterations only in responsive tumors (ptW, ptAB, and ptH) and not in nonresponders (ptD and ptAM) (Fig. 6). The direction of

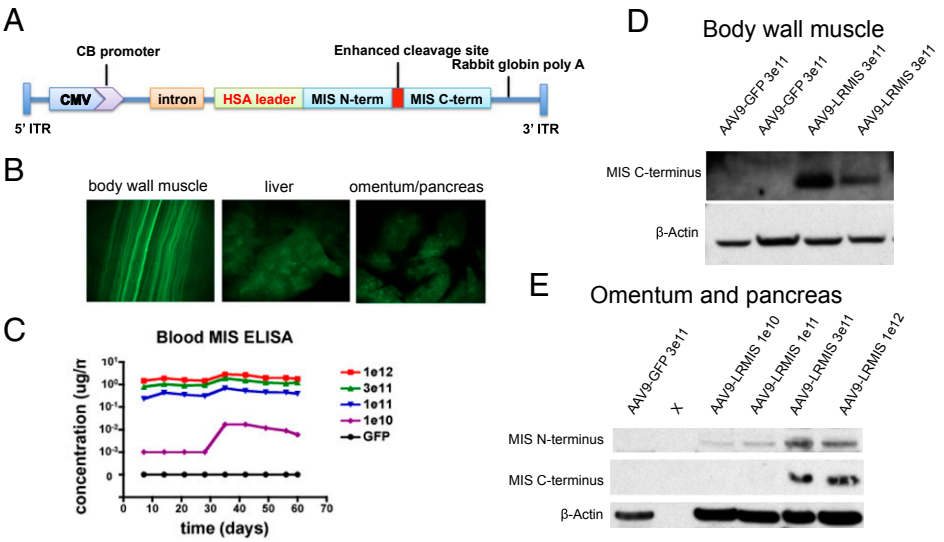

Fig. 4. AAV9-LRMIS virus administered i.p. into mice infects body wall muscles and some peritoneal organs, which result in sustained expression of the transgene and secretion into the blood. (*A*) The AAV9 vector expressed LRMIS containing the albumin leader sequence and the enhanced cleavage site. (*B*) Micrographs of GFP expression in the body wall muscle, liver, and omentum/pancreas of Nu/Nu mice 60 d after infection with 3E11 AAV9-GFP taken with 8× magnification. (*C*) MIS measured in serum by ELISA after infection of Nu/Nu mice with escalating doses of AAV9-LRMIS (1E10, 1E11, 3E11, and 1E12) or AAV9-GFP over 60 d. Western blot of protein lysates from (*D*) body wall muscle or (*E*) omentum and pancreas 60 d after injection of Nu/Nu mice with 3E11 AAV9-LRMIS that were probed with anti-MIS antibody or loading control (β-actin). CB, chicken beta-actin; HSA, human serum albumin; ITR, inverted terminal repeat.

the response measured at the time of tumor takedown (down-regulation of P21 and P-SMAD1,5,8) in ptAB differed from the canonical response (up-regulation of P21 and P-SMAD1,5,8) observed in ptW and ptH. Tumor histologies at the endpoint in AAV9 control or AAV9-LRMIS in the responsive PDXas (ptW, ptAB, and ptH) were similar.

MISR2 Is Expressed in High-Grade Serous Epithelial Ovarian Cancer Tumors with High Frequency but Does Not Correlate with Prognosis. A tissue microarray (TMA) of 416 formalin-fixed, paraffin-embedded, high-grade serous ovarian tumors cores from 205 patients with two independent intact cores and 5 patients with only one core was immunohistochemically stained for MISRII and

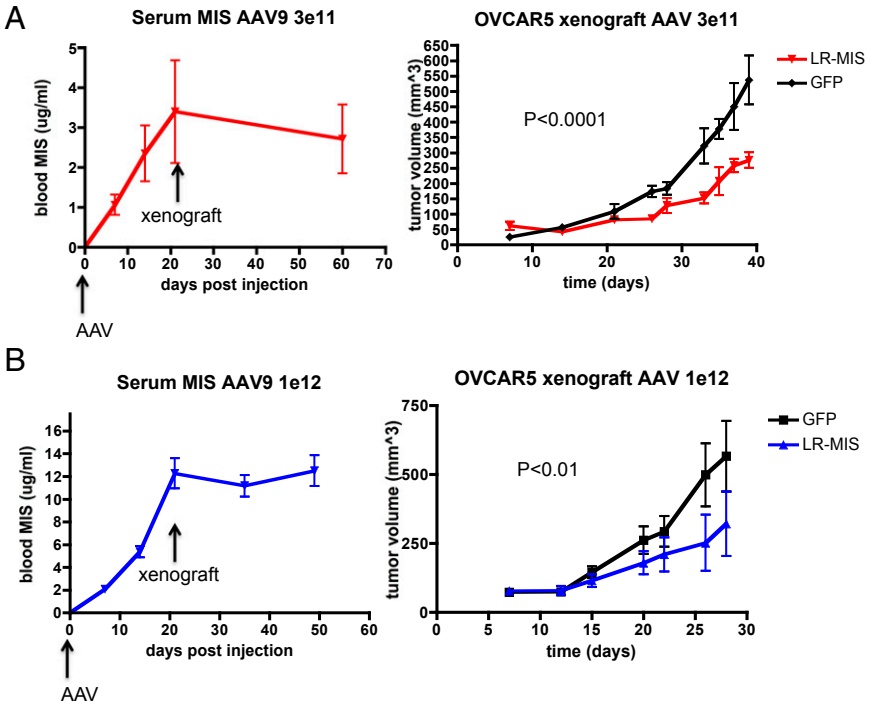

Fig. 5. AAV9-LRMIS pretreatment results in elevated levels of MIS at the time of engraftment and inhibition of OVCAR5 xenograft tumor growth. Pretreatment with either (*A*) 3E11 or (*B*) 1E12 particles of AA9-LRMIS or AAV9-GFP control 3 wk before engraftment of 5 million OVCAR5 cells s.c. in the flank of Nu/Nu (groups of five) mice results in (*Left*) elevated blood levels of MIS by ELISA and (*Right*) inhibition of tumor growth as determined by two times per week measurement with calipers. Tumor volume [$V = (L \times W \times W)/2$] growth was analyzed by two-way ANOVA.

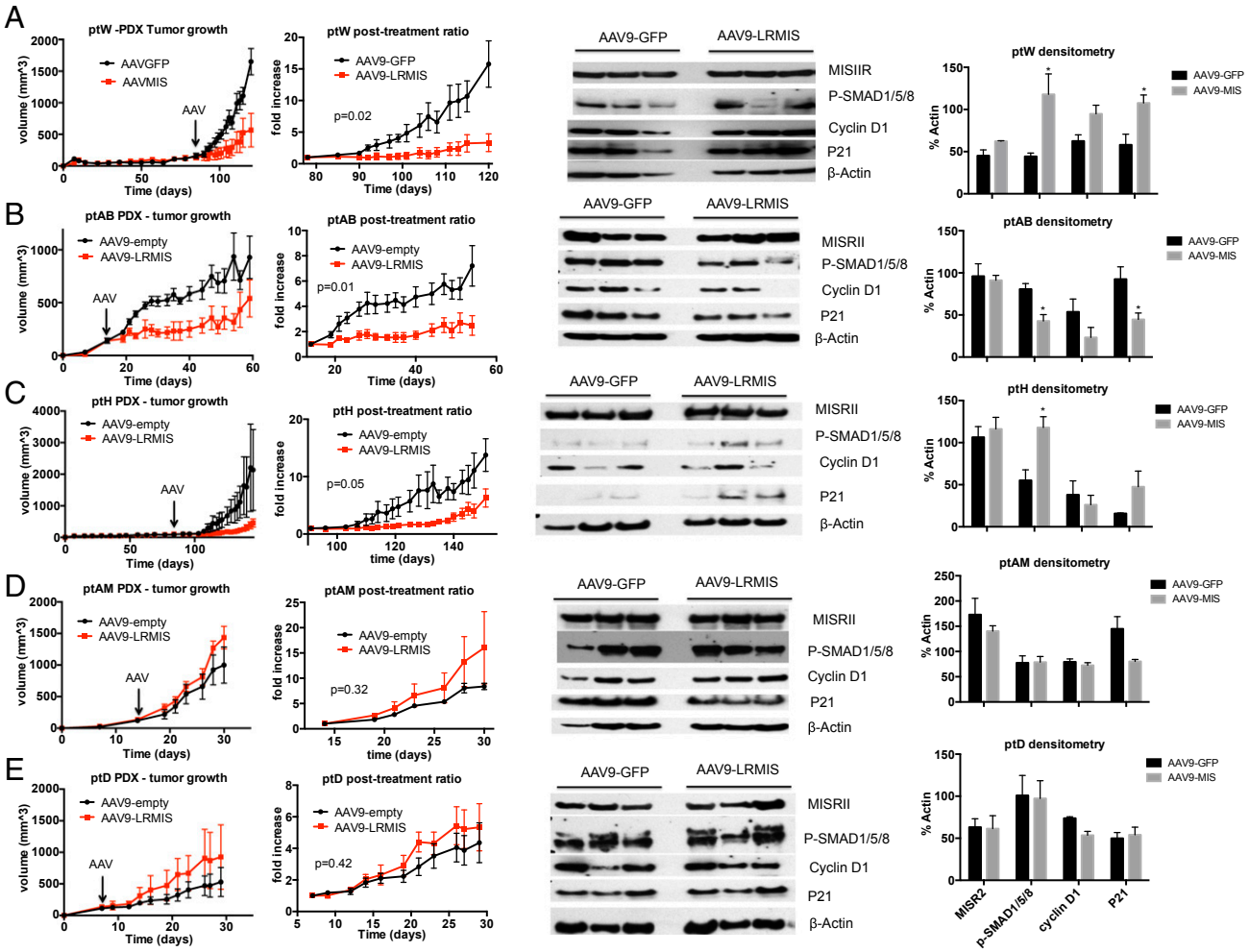

Fig. 6. Tumor volume growth and marker expression of patient-derived xenografts after treatment with AAV9-LRMIS; 5 M cells of (*A*) ptW, (*B*) ptAB-sph, (*C*) ptH, and (*D*) ptAM-sph were xenografted into NOD/SCIDγ mice ($n = 10$), and 5 M cells of (*E*) ptD were xenografted into Nude mice. Tumors were allowed to grow to an average size of 100 mm^3. Mice were then treated with 3E11 of AAV9-GFP control ($n = 5$) or AAV9-LRMIS ($n = 5$; arrows). Tumor volume was measured by calipers weekly, and mean tumor growth was plotted (±SEM; column 1). Statistical comparisons of the control and treatment curves were performed by two-way ANOVA from the day of treatment, showing relative graft size ratio until endpoint (column 2). Representative tumor lysates of three treated and three control animals at endpoint were analyzed by Western blot for expression of MISRII, P-SMAD1/5/8, cyclin D1, P21, and β-actin control (column 3), and relative expression was quantified by densitometry (normalized to loading control) where statistical significance (denoted by asterisks) was inferred by *t* test with $P < 0.05$ (column 4).

matched to clinical information (Table S1). The median age of the patient population at diagnosis was 61.5 y (32.6–91.3 y); at the time of this analysis, 132 (64.3%) patients has succumbed to the disease. The overall survival of those patients from time of diagnosis ranged from 10 to 4,655 d, with a median survival of 900 d and an average survival of 1,078 ± 882 d. The International Federation of Gynecology and Obstetrics staging breakdown of the patient population was stages II (1.4%), IIIA/B (21.4%), IIIC (49%), and IV (20.9%) and unknown (7.6%), whereas the grading was scored as grade 2 (10.9%) or 3 (89.1%).

To estimate the proportion of patients with high-grade serous ovarian cancer-bearing MISRII-positive tumors, TMAs were stained with an immunohistochemistry (IHC)-compatible MISRII antibody that selectively stained, as positive controls, granulosa cells of growing follicles in rat ovaries as well as Sertoli cells lining seminiferous tubules of prepubertal mouse testes (Fig. 7*A*). The staining intensity of the cores was scored as negative (−), weakly positive (+), moderately positive (++), or strongly positive (+++) (Fig. 7*B*) by two independent observers blinded to clinical information. Because 205 patients had two representative tumor cores, we could compare intensity in each of the pairs and found that only 11.7% of patients ($n = 24$) had two negative tumor cores, whereas 88.3% of patient had at least one core with some MISRII staining (Table S2). The majority of patients (65.4%; $n = 134$) had tumors with significant MISRII staining, with at least one core being moderately positive or strongly positive. Expression of MISRII was restricted to the epithelial cancer cells staining both the cytoplasm and cell membranes homogeneously throughout each tumor core.

To confirm scoring using an unbiased evaluation of MISRII staining, the TMA slides were scanned, digitized, and analyzed using the Aperio image analysis software. We derived a positivity intensity score by multiplying the positivity score (positive pixels per total pixels) as a measure of the proportion of the tumor stained by the intensity score, a measure of the strength of the stain. Patients were stratified by positivity intensity score, and the upper and lower quartiles of MISRII expressers were compared and found to be highly significantly different ($P < 0.0001$) (Fig. 7*C*). Using this classification scheme, we find that there is no statistically significant difference in overall survival between

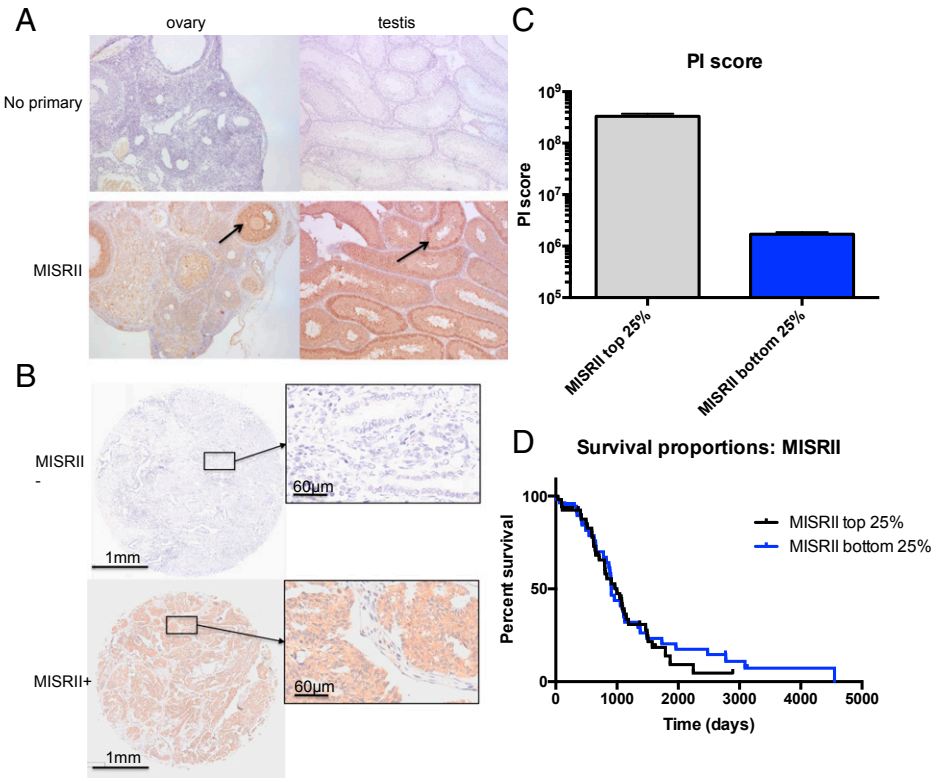

Fig. 7. TMAs of 205 ovarian tumors of high-grade histotype serous stained for MISRII expression by immunohistochemistry. (*A*) MISRII antibody stained specifically granulosa cells (arrow) in rat ovaries and Sertoli cells (arrow) in mouse testes, with no observed background in those same tissues stained with only secondary HRP-conjugated antibody (no primary). (*B*) Representative tumor cores from the TMA with negative or positive staining for MISRII. (*C*) Unbiased image analysis of positive and negative tumor cores comparing MISRII staining intensity [positivity intensity (PI) score] in upper and lower quartiles of patients as analyzed by Scanscope software ($P < 0.0001$). (*D*) Kaplan–Meier survival analysis of upper and lower quartiles of patients stratified by MISRII expression by Scanscope software of the TMA ($P = 0.61$).

MISRII upper quartile and MISRII lower quartile of patients as evidenced by the Kaplan–Meier curves (Fig. 7*D*); median survival of patients in the top 25% of expressers was 999 d vs. 907 d for the bottom 25%.

Discussion

A substantial number of studies has shown the benefit of MIS treatment in vivo using both murine and established human ovarian cancer cell line xenografts treated with recombinant MIS protein. However, limited availability of potent and stable protein had prevented empirical testing of the response rate to MIS in vivo in ovarian cancer, particularly in the platinum-resistant, high-grade serous histotype. Attesting to the importance of evaluating MIS in this particular subgroup is the evidence that MIS targets the stem-enriched population to which chemoresistant recurrence has been attributed (11, 15, 21). One of the aims of this study is to determine the potential for response by examining the prevalence of receptor expression (MISRII) in primary cell lines derived from ascites, PDXa, and high-grade serous ovarian cancer tumors using TMAs. Furthermore, MIS response was evaluated in vitro using spheroid assays in a panel of primary ascites cell lines capable of suspension growth as well as in vivo through the establishment of PDXa tumor growth models treated with gene therapy to deliver high and sustained levels of a potent MIS analog (LRMIS) in an AAV9.

The recent development of PDXs, in which small pieces of undigested primary tumors are serially passaged in immunocompromised mice, has ushered in a new era of precision medicine, where mice function as avatars to evaluate patient-specific therapies (22–26). Some of the limitations of PDXas are the serial passaging of the tumors, which can be lengthy and cause loss of clonal diversity, and replacement of human stroma and human vasculature (27, 28). Methods that establish primary cell lines and PDXas in parallel allow for faster in vivo and in vitro testing that could direct therapeutic strategies for individual patients in real time (19, 29–32), making ascites an ideal source of material for xenografts, which we distinguished from biopsy PDXs by referring to them as PDXas. Ascites can be obtained less invasively throughout the clinical course of the disease (33), are abundant and amenable to direct engraftment in a large number of mice, and often grow in tissue culture, allowing for parallel in vitro analyses. We have optimized this source of ovarian cancer cells to test the responsiveness and mechanisms of MIS sensitivity by deriving both short-term primary cell lines and PDXas, specifically from the patient population with the recurrent platinum-resistant, high-grade serous phenotype. Cell lines were also grown both as monolayers in serum-containing media and in suspension cultures in serum-free spheroid media (Fig. 1), the latter of which has been imputed to preserve the cancer stem cell phenotype (34, 35). The success rate of in vitro primary culture, however, is limited by the incidence of malignant cells within ascites; in monolayer cultures, 38.3% of ascites generated cell lines, whereas the addition of spheroid culture conditions incrementally increased our total success rate to 56.5%. Of these cell lines, 50% (Table 1) readily formed tumors s.c. in NOD/SCID/IL2Rγ Jaxx mice (36), from which we screened MIS responsiveness in a panel of five PDXa models (Fig. 6) with the most favorable untreated growth.

When matched cell lines grown in adherent or suspension cultures were compared, spheroids had generally increased expression

of pluripotency factors (Fig. 3*A*), making them ideally suited to test the effect of MIS on stem/progenitor-enriched cell populations (11, 15). In a spheroid in vitro growth assay, four of six primary lines displayed significant growth inhibition by MIS at 5 μg/mL compared with controls (Fig. 3*B*). This panel of six spheroid cell lines all expressed essential pathway components necessary for MIS signal transduction, such as MISRII by Western blot and qPCR and the type I receptors (ALK2, ALK3, and ALK6) and the SMADs (SMAD1, SMAD4, SMAD5, and SMAD8/9) by qPCR (Fig. 3*C*). Interestingly, two of the primary spheroid cell lines (ptAM and ptAB) did not express SMAD8/9 or the inhibitory SMAD6, which did not seem to affect the MIS responsiveness.

We used a gene therapy approach based on AAV9 to deliver LRMIS (16) in PDXa models as a feasible way to determine the percentage of patients responsive to MIS. The AAV9 serotype of the AAV family has been safely used to infect a range of cells and tissues, including cardiac myocytes (37), lung tissue (38), and neurons of the CNS and peripheral nervous system (17, 39–43), to correct a host of genetic diseases, including ALS (39, 40, 43), Parkinson's (44), Huntington's (45–51), and Sandoff (52). AAV9 has been shown to have enhanced tropism to muscles and neurons, high infectivity, and stable long-term expression, making it ideally suited for the treatment of tumors, where normal infected tissues (e.g., muscles) serve as a bioreactor-like source of therapeutic protein for long-term secretion into the circulation (53). To date, AAV9 has not been evaluated for the treatment of cancer, and AAVs, in general, have been underused in treating ovarian cancer, with the exceptions of AAVrh.10 delivering Bevacizumab (54) and AAV2 delivering Kringle 5 (55) or endostatin (56). The tropism of AAV9 delivered i.p., as evidenced by AAV9-GFP infecting the body wall muscle, omentum, (Fig. 4*B*), and gut mesentery, underscores its suitability for the treatment of ovarian cancers, which frequently metastasize to the latter two sites. Furthermore, neither AAV9 infection nor sustained LRMIS expression resulted in overt measurable toxicity on acute and chronic exposures, predicting a good safety profile. AAVs have been shown to be effective and well-tolerated in primates for over 9 y (53), and they have been approved for clinical use (57–59). Furthermore, the levels of MIS reached in the mice treated with AAV9-LRMIS in this study are equivalent to those observed in normal baby boys (60), further supporting its potential safety profile in humans.

A single injection of AAV9-LRMIS resulted in significant inhibition of tumor growth as a pretreatment model with OVCAR5 as well as a posttreatment of palpable tumors in three of five PDXas, which it must be remembered were derived from patients who had failed all previous therapeutic interventions. Because all five PDXa tumors express the MISRII receptor as well as the downstream molecular machinery necessary for response, receptor detection may not be sufficient to predict responsiveness. In vivo response was accompanied with significant changes measured at tumor takedown in phosphorylation of SMAD1, SMAD5, and SMAD8 (61, 62) and expression levels of cyclins (cyclin D1) and cyclin-dependent kinase (P21) in the tumors of AAV9-LRMIS–treated animals (Fig. 6), suggesting that successful MIS treatment results in cell cycle disruption, which is in accordance with previous reports (15, 63). In ptAB, treatment with AAV9-LRMIS paradoxically down-regulated P-SMAD1, P-SMAD5, P-SMAD8, and P21, suggesting a different mechanism of action in this PDXa that does not express SMAD8/9 or SMAD6. The interpretation of these data must take into account the fact that expression of these proteins was measured in the tumors only at the endpoint after continuous long-term exposure to high-MIS levels, which can only capture changes at equilibrium. The observation that ptAB also did not respond to MIS in vitro in the spheroid growth assay suggests that some of the contributing mechanisms of action may be non cell-autonomous, such as inhibition of angiogenesis. The heterogeneity of these data suggests that patients tumors should be evaluated individually in future studies aimed at elucidating gene expression response to MIS.

Immunohistochemistry of a TMA consisting of fixed high-grade serous tumor cores from 210 patients revealed that 88% displayed at least one core staining positive for MISRII and 65% had at least one core staining medium or strong. These results are in agreement with previous reports indicating that a majority (69%) of mixed histotype epithelial ovarian cancers express MISRII in TMAs (64), with the highest expressers consisting of serous (76% of $n = 29$) and mucinous (100% of $n = 3$) histotypes. We previously reported that 88.9% of cytokeratin-positive ovarian cancer ascites cells that bind biotinylated MIS protein also expressed MISRII by RT-PCR (65). It is important to note that MISRII is also expressed in normal adult tissues, such as male and female gonads (60), brain (66–70), and motor neurons (71), where the latter is known to be salutory, highlighting the importance for exercising caution when choosing to target MISRII therapeutically; we consider delivery of the natural ligand to be the ideal modality. Recent evidence of intracellular accumulation of MISRII also raises questions about the relative availability of MISRII to ligand binding in cancer cells and may indicate complex regulation or other cytoplasmic functions, which have contributions to the antitumorigenic response which remain unknown (72).

The ability to evaluate MIS response both in vivo with PDXa to AAV9-delivered MIS and in vitro with matched primary cell lines will allow us to investigate the panoply of molecular mechanisms influencing responsiveness, identify biomarkers predictive of response, and test other therapies combined with MIS. Furthermore, AAV9 is a promising gene therapy vector, with use in ovarian cancer that could be expanded to deliver other rationally chosen protein therapeutics.

Materials and Methods

Ascites Cell Line Generation. All deidentified ascites samples were collected after informed consent under Institutional Review Board-approved protocols (2007P001918/Massachusetts General Hospital). Freshly collected ascites were aliquoted in 500-mL conical centrifuge tubes and spun at 1,780 × *g* for 25 min. Some supernatant was reserved (100 mL) and frozen at −80 °C. The cell pellet was washed one time in PBS and incubated for 5 min on ice in 10 volumes ammonium-chloride-potassium buffer (Life Technologies) to lyse RBCs; cells were then spun down and resuspended in PBS, and the process was repeated until RBC lysis was complete. The nucleated cell pellet, which may contain immune cells, fibroblasts, mesothelial cells, and cancer cells, was introduced into tissue culture under two different conditions (adherent and nonadherent) and preserved in liquid nitrogen (Fig. 1). Each deidentified patient was assigned a letter code (A–AZ), which was used to identify the primary cell line (e.g., ptD). The suffix spheroid (-sph) was given to the primary cell lines grown in suspension as spheroids (in serum-free media) to distinguish from adherent cultures (in serum-containing media; e.g., ptAB-sph vs. ptAB). Low passages of both the adherent and suspension cultured cell lines were used in vitro and in vivo for experiments or frozen in liquid nitrogen for future use.

MIS Protein Purification. The purification of human recombinant LRFMIS was performed as previously described (16). Briefly, commercially available anti-FLAG M2 (Sigma-Aldrich) immunoaffinity beads were incubated with conditioned media from a CHO clone expressing LRFMIS overnight. The beads were centrifuged and washed five times in Tris-buffered saline (Boston Bioproducts). MIS was eluted from the beads with 1 volume 3× flag peptide (Sigma-Aldrich), with a purification yield of ∼35%. Identically prepared elutions from beads incubated with untransfected CHO-conditioned media were used as mock-purified controls for use in the in vitro experiments.

Spheroid Assay. Small nascent cancer cell spheroids were collected 1 wk after dissociation and passage of suspension cultures of primary ovarian cancer cells. A single spheroid was deposited in each well of a round-bottomed 96-well plate in 100 μL stem cell media. LRFMIS (5 μg/mL final) and control mock elution in equal volume were mixed in spheroid media, and a 100-μL volume was gently added to each well. Sphere length (*L*) and width (*W*) were measured two to three times per week to calculate volume (*V*) by the following

equation: $V = (L \times W \times W)/2$. In spheroid assays maintained for over 2 wk, 100 μL media were gently removed to avoid sphere dissociation and replaced with new media containing appropriate concentrations of drug. At least eight spheroids were monitored, measured, and plotted for each group, and experiments were repeated at least three times.

AAV9-LRMIS Preparation and Use. Because purification was not necessary, LRMIS vectors without the Flag were used for all in vivo experiments. The gene expression cassette in the rAAV genome consists of a CMV enhancer/chicken β-actin promoter driving the human LRMIS cDNA followed by a rabbit β-globin polyadenylation signal. The entire gene expression cassette is flanked by AAV2 inverted terminal repeats serving as packaging signals.

rAAV vectors were produced and titrated as previously described (73). Briefly, HEK293 cells were transfected with the plasmids harboring the inverted terminal repeat-flanked human LRMIS construct, expressing AAV9 capsid proteins and adenoviral helper proteins, respectively. rAAVs were harvested and purified by cesium chloride sedimentation and dialysis. rAAV vector titer was determined by qPCR of genome copy and silver staining of capsid proteins.

Cancer Cell Xenografts in Mice. All animal experiments were approved and carried out in accordance with a Massachusetts General Hospital Institutional Animal Care and Use Committee approved experimental protocol (2009N000033).

For the OVCAR5 xenografts, Nu/Nu mice were injected with either 3E11 ($n = 10$) or 1E12 ($n = 10$) virions of AAV9-LRMIS or AAV9-GFP controls; 3 wk after AAV9 injection, 5 M OVCAR5 cells resuspended in Matrigel (single batch; Corning) were implanted s.c. in the flank of the pretreated mice.

For the PDXa, low-passage (three to five) primary patient cell lines grown as either monolayers (ptD, ptH, and ptW) or spheroids (ptAB-sph and ptAM-sph) were implanted s.c. into NOD/SCID/IL2Rγ Jaxx mice (Jackson Laboratory). For each PDXa group, 5 M cells resuspended in Matrigel (single batch; Corning) were implanted s.c. in the flank of 10 mice, and tumor growth was monitored two times per week by caliper measurements. When the average tumor size exceeded 100 mm^3 (~4.8-mm diameter), the mice were treated with 3E11 virions of AAV9-LRMIS ($n = 5$ for each patient's tumor) or AAV9 empty vector ($n = 5$).

Tumor growth was monitored two times per week by caliper measurements of length (L) and width (W), from which tumor volume (V) was estimated using the following formula: $V = (L \times W \times W)/2$. The studies ended when at least one mouse reached endpoint, which consisted of either tumor ulceration or tumor diameter exceeding 20 mm. Blood and tumor samples were collected at endpoint, fixed, and/or frozen.

Western Analysis.

Cell lines. Total protein lysates were prepared from cell pellets harvested from primary ascites cell lines and the human ovarian cancer cell line (OVCAR5) and separated by NuPage (Novex Life Tech) 4–12% (wt/wt) gel electrophoresis. Membranes were incubated overnight at 4 °C with rabbit anti-MISR2 antibody (H150; Santa Cruz) at 1:500 dilution and then, incubated for 1 h at room temperature with secondary antibody at 1:10,000 dilution of anti-rabbit HRP (Cell Signaling Technology).

Tumor lysates. At xenograft endpoint, total protein lysates were prepared from tumor pieces mechanically disrupted using a handheld pestle. Primary antibodies used were CyclinD1 diluted 1:250 (Cell Signaling), MISRII (H-150) at 1:500 (Santa Cruz), p21 at 1:1,000 (Santa Cruz), and pSMAD1/5/8 at 1:500 (Cell Signaling Technology).

qPCR. qPCR was performed on primary cell lines established from patient ascites or the ovarian cancer cell line OVCAR5. Primers were designed to span exon–exon junctions for the target genes (MISRII, ALK2, ALK3, ALK6, SMAD1, SMAD4, SMAD5, SMAD6, SMAD9, SMURF1, and SMURF2) using GAPDH as an internal standard (Table S3). Relative expression was calculated using cycle threshold (Ct) values by $2^{-\Delta Ct}$, and statistical analysis was performed using Prism software (Graphpad).

Human MIS ELISA Assay. ELISAs were performed to measure circulating human MIS in the serum of treated animals as previously reported (16, 74). Blood was collected at interval time points after treatment and at endpoint through either saphenous or facial venipuncture, and it was placed into heparinized Microvette tubes (Sarsthedt) or BD Microtainer.

TMA of Ovarian Serous Adenocarcinoma. In total, 416 formalin-fixed, paraffin-embedded, microdissected tumor cores of 3-mm diameter with >80% tumor and <20% necrosis/stroma were collected under institutional review board-approved protocols (MGH2007P00001918 or DFCI 02–051) from ovarian cancer patients hospitalized at Massachusetts General Hospital between 1993 and 2009 as previously described (75). TMA slides were incubated with an anti-MISRII antibody (R&D) at a concentration of 5 μg/mL (1:40) followed by incubation with a donkey anti-sheep HRP (R&D) secondary at a concentration of 1:400. Slides were scanned and digitized with an Aperio Scanscope (Leica), and they were analyzed with the Aperio Imagescope (Leica) imaging software. Intensity scores were calculated as the product of stained area fraction (positivity) and intensity (total intensity of cores stained positive). Overall survival and progression-free survival were analyzed by Kaplan–Meier plots, and statistical significance was inferred by log rank tests. Comparisons of incidence of various clinical parameters in each group were done using χ^2 analysis. Statistical analyses were performed using the Prism 6 software (Graphpad).

ACKNOWLEDGMENTS. We thank Dorothy Ndishabandi for help scanning the tissue microarray slides and Jingwen Chen for her instrumental role in coordinating and collecting ascites samples in Interventional Radiology. This study was funded, in part, by an Ann Shreiber Mentored Investigator Grant from the Ovarian Cancer Research Fund (to D.P.); the Sudna Gar Fellowship (to D.P.); an Innovation Development Award from Massachusetts General Hospital, Partners Healthcare (to D.P. and P.K.D.); Department of Defense Translational Pilot Award OC110078 (to P.K.D.); NIH Grant R01CA17393 (to P.K.D.); a Massachusetts General Hospital Department of Surgery Award (to P.K.D.); philanthropy from the Austen Fund, the McBride family, and Commons Development (P.K.D.); and royalties from the use of the Mullerian inhibiting substance ELISA in infertility clinics around the world.

1. Burger RA, et al.; Gynecologic Oncology Group (2011) Incorporation of bevacizumab in the primary treatment of ovarian cancer. *N Engl J Med* 365(26):2473–2483.
2. Perren TJ, et al.; ICON7 Investigators (2011) A phase 3 trial of bevacizumab in ovarian cancer. *N Engl J Med* 365(26):2484–2496.
3. Ledermann J, et al. (2012) Olaparib maintenance therapy in platinum-sensitive relapsed ovarian cancer. *N Engl J Med* 366(15):1382–1392.
4. Scully RE (1977) Ovarian tumors. A review. *Am J Pathol* 87(3):686–720.
5. Lee MM, et al. (1997) Measurements of serum müllerian inhibiting substance in the evaluation of children with nonpalpable gonads. *N Engl J Med* 336(21):1480–1486.
6. Cate RL, et al. (1986) Isolation of the bovine and human genes for Müllerian inhibiting substance and expression of the human gene in animal cells. *Cell* 45(5):685–698.
7. Lorenzo HK, et al. (2002) New approaches for high-yield purification of Müllerian inhibiting substance improve its bioactivity. *J Chromatogr B Analyt Technol Biomed Life Sci* 766(1):89–98.
8. Ragin RC, Donahoe PK, Kenneally MK, Ahmad MF, MacLaughlin DT (1992) Human müllerian inhibiting substance: Enhanced purification imparts biochemical stability and restores antiproliferative effects. *Protein Expr Purif* 3(3):236–245.
9. Connolly DC, et al. (2003) Female mice chimeric for expression of the simian virus 40 TAg under control of the MISIIR promoter develop epithelial ovarian cancer. *Cancer Res* 63(6):1389–1397.
10. Pieretti-Vanmarcke R, et al. (2006) Recombinant human Mullerian inhibiting substance inhibits long-term growth of MIS type II receptor-directed transgenic mouse ovarian cancers in vivo. *Clin Cancer Res* 12(5):1593–1598.
11. Wei X, et al. (2010) Mullerian inhibiting substance preferentially inhibits stem/progenitors in human ovarian cancer cell lines compared with chemotherapeutics. *Proc Natl Acad Sci USA* 107(44):18874–18879.
12. Stephen AE, et al. (2001) Tissue-engineered cells producing complex recombinant proteins inhibit ovarian cancer in vivo. *Proc Natl Acad Sci USA* 98(6):3214–3219.
13. Stephen AE, et al. (2002) Highly purified müllerian inhibiting substance inhibits human ovarian cancer in vivo. *Clin Cancer Res* 8(8):2640–2646.
14. Szotek PP, et al. (2006) Ovarian cancer side population defines cells with stem cell-like characteristics and Mullerian Inhibiting Substance responsiveness. *Proc Natl Acad Sci USA* 103(30):11154–11159.
15. Meirelles K, et al. (2012) Human ovarian cancer stem/progenitor cells are stimulated by doxorubicin but inhibited by Mullerian inhibiting substance. *Proc Natl Acad Sci USA* 109(7):2358–2363.
16. Pépin D, et al. (2013) An albumin leader sequence coupled with a cleavage site modification enhances the yield of recombinant C-terminal Mullerian Inhibiting Substance. *Technology (Singap)* 1(1):63–71.
17. Gao G, Mueller C, Flotte TR (2010) AAV as a gene therapy vector. *Regenerative Therapy for the Musculoskeletal System Using Recombinant Adeno-Associated Viral Vectors*, ed Madry MCH (Research Signpost, Kerala, India), pp 1–21.
18. Scott CL, Becker MA, Haluska P, Samimi G (2013) Patient-derived xenograft models to improve targeted therapy in epithelial ovarian cancer treatment. *Front Oncol* 3:295.
19. Dobbin ZC, et al. (2014) Using heterogeneity of the patient-derived xenograft model to identify the chemoresistant population in ovarian cancer. *Oncotarget* 5(18):8750–8764.
20. Gao GP, et al. (2002) Novel adeno-associated viruses from rhesus monkeys as vectors for human gene therapy. *Proc Natl Acad Sci USA* 99(18):11854–11859.
21. Gupta PB, et al. (2009) Identification of selective inhibitors of cancer stem cells by high-throughput screening. *Cell* 138(4):645–659.

22. Elkas JC, et al. (2002) A human ovarian carcinoma murine xenograft model useful for preclinical trials. *Gynecol Oncol* 87(2):200–206.
23. Repasky EA, Tims E, Pritchard M, Burd R (1999) Characterization of mild whole-body hyperthermia protocols using human breast, ovarian, and colon tumors grown in severe combined immunodeficient mice. *Infect Dis Obstet Gynecol* 7(1-2):91–97.
24. Topp MD, et al.; Australian Ovarian Cancer Study (2014) Molecular correlates of platinum response in human high-grade serous ovarian cancer patient-derived xenografts. *Mol Oncol* 8(3):656–668.
25. Weroha SJ, et al. (2014) Tumorgrafts as in vivo surrogates for women with ovarian cancer. *Clin Cancer Res* 20(5):1288–1297.
26. Xu Y, et al. (1999) Characterization of human ovarian carcinomas in a SCID mouse model. *Gynecol Oncol* 72(2):161–170.
27. Hylander BL, et al. (2013) Origin of the vasculature supporting growth of primary patient tumor xenografts. *J Transl Med* 11:110.
28. Sivanathan L, Chow A, Wong A, Hoang VC, Emmenegger U (2014) In vivo passage of human prostate cancer cells in mice results in stable gene expression changes affecting numerous cancer-associated biological processes. *Prostate* 74(5):537–546.
29. Arend RC, et al. (2014) Inhibition of Wnt/β-catenin pathway by niclosamide: A therapeutic target for ovarian cancer. *Gynecol Oncol* 134(1):112–120.
30. Bradley A, et al. (2014) EDD enhances cell survival and cisplatin resistance and is a therapeutic target for epithelial ovarian cancer. *Carcinogenesis* 35(5):1100–1109.
31. Crystal AS, et al. (2014) Patient-derived models of acquired resistance can identify effective drug combinations for cancer. *Science* 346(6216):1480–1486.
32. Fauci JM, et al. (2014) Monoclonal antibody-based immunotherapy of ovarian cancer: Targeting ovarian cancer cells with the B7-H3-specific mAb 376.96. *Gynecol Oncol* 132(1):203–210.
33. Létourneau IJ, et al. (2012) Derivation and characterization of matched cell lines from primary and recurrent serous ovarian cancer. *BMC Cancer* 12:379.
34. Lee JW, Na DS, Kang JY, Lee SH, Ju BK (2006) Differentiation of mouse p19 embryonic carcinoma stem cells injected into an empty zebrafish egg chorion in a microfluidic device. *Biosci Biotechnol Biochem* 70(6):1325–1330.
35. Liao J, et al. (2014) Ovarian cancer spheroid cells with stem cell-like properties contribute to tumor generation, metastasis and chemotherapy resistance through hypoxia-resistant metabolism. *PLoS One* 9(1):e84941.
36. Shultz LD, et al. (2005) Human lymphoid and myeloid cell development in NOD/LtSz-scid IL2R gamma null mice engrafted with mobilized human hemopoietic stem cells. *J Immunol* 174(10):6477–6489.
37. Chaanine AH, et al. (2014) Effect of bortezomib on the efficacy of AAV9.SERCA2a treatment to preserve cardiac function in a rat pressure-overload model of heart failure. *Gene Ther* 21(4):379–386.
38. Gubrij IB, Martin SR, Pangle AK, Kurten R, Johnson LG (2014) Attenuation of monocrotaline-induced pulmonary hypertension by luminal adeno-associated virus serotype 9 gene transfer of prostacyclin synthase. *Hum Gene Ther* 25(6):498–505.
39. Duque S, et al. (2009) Intravenous administration of self-complementary AAV9 enables transgene delivery to adult motor neurons. *Mol Ther* 17(7):1187–1196.
40. Foust KD, et al. (2009) Intravascular AAV9 preferentially targets neonatal neurons and adult astrocytes. *Nat Biotechnol* 27(1):59–65.
41. McCown TJ (2005) Adeno-associated virus (AAV) vectors in the CNS. *Curr Gene Ther* 5(3):333–338.
42. Mi J, et al. (1999) Recombinant adeno-associated virus (AAV) drives constitutive production of glutamate decarboxylase in neural cell lines. *J Neurosci Res* 57(1): 137–148.
43. Zhang H, et al. (2011) Several rAAV vectors efficiently cross the blood-brain barrier and transduce neurons and astrocytes in the neonatal mouse central nervous system. *Mol Ther* 19(8):1440–1448.
44. Kermer P, et al. (2015) BAG1 is neuroprotective in in vivo and in vitro models of Parkinson's disease. *J Mol Neurosci* 55(3):587–595.
45. Crook ZR, Housman DE (2013) In vivo identification of therapeutic constructs from pooled candidates in HD model mice. *J Huntingtons Dis* 2(4):437–441.
46. Dufour BD, Smith CA, Clark RL, Walker TR, McBride JL (2014) Intrajugular vein delivery of AAV9-RNAi prevents neuropathological changes and weight loss in Huntington's disease mice. *Mol Ther* 22(4):797–810.
47. Franich NR, et al. (2008) AAV vector-mediated RNAi of mutant huntingtin expression is neuroprotective in a novel genetic rat model of Huntington's disease. *Mol Ther* 16(5):947–956.
48. McBride JL, et al. (2003) Structural and functional neuroprotection in a rat model of Huntington's disease by viral gene transfer of GDNF. *Exp Neurol* 181(2):213–223.
49. Ramaswamy S, Kordower JH (2012) Gene therapy for Huntington's disease. *Neurobiol Dis* 48(2):243–254.
50. Ramaswamy S, et al. (2009) Intrastriatal CERE-120 (AAV-Neurturin) protects striatal and cortical neurons and delays motor deficits in a transgenic mouse model of Huntington's disease. *Neurobiol Dis* 34(1):40–50.
51. Southwell AL, Ko J, Patterson PH (2009) Intrabody gene therapy ameliorates motor, cognitive, and neuropathological symptoms in multiple mouse models of Huntington's disease. *J Neurosci* 29(43):13589–13602.
52. Walia JS, et al. (2015) Long-term correction of sandhoff disease following intravenous delivery of rAAV9 to mouse neonates. *Mol Ther* 23(3):414–422.
53. Rivera VM, et al. (2005) Long-term pharmacologically regulated expression of erythropoietin in primates following AAV-mediated gene transfer. *Blood* 105(4): 1424–1430.
54. Xie Y, et al. (2014) AAV-mediated persistent bevacizumab therapy suppresses tumor growth of ovarian cancer. *Gynecol Oncol* 135(2):325–332.
55. Bui Nguyen TM, Subramanian IV, Xiao X, Nguyen P, Ramakrishnan S (2010) Adeno-associated virus-mediated delivery of kringle 5 of human plasminogen inhibits orthotopic growth of ovarian cancer. *Gene Ther* 17(5):606–615.
56. Subramanian IV, Ghebre R, Ramakrishnan S (2005) Adeno-associated virus-mediated delivery of a mutant endostatin suppresses ovarian carcinoma growth in mice. *Gene Ther* 12(1):30–38.
57. Ferreira V, Petry H, Salmon F (2014) Immune esponses to AAV-vectors, the glybera example from bench to bedside. *Front Immunol* 5:82.
58. Ferreira V, et al. (2014) Immune responses to intramuscular administration of alipogene tiparvovec (AAV1-LPL(S447X)) in a phase II clinical trial of lipoprotein lipase deficiency gene therapy. *Hum Gene Ther* 25(3):180–188.
59. Salmon F, Grosios K, Petry H (2014) Safety profile of recombinant adeno-associated viral vectors: Focus on alipogene tiparvovec (Glybera®). *Expert Rev Clin Pharmacol* 7(1):53–65.
60. Lee MM, et al. (1996) Mullerian inhibiting substance in humans: Normal levels from infancy to adulthood. *J Clin Endocrinol Metab* 81(2):571–576.
61. Clarke TR, et al. (2001) Müllerian inhibiting substance signaling uses a bone morphogenetic protein (BMP)-like pathway mediated by ALK2 and induces SMAD6 expression. *Mol Endocrinol* 15(6):946–959.
62. Zhan Y, et al. (2006) Müllerian inhibiting substance regulates its receptor/SMAD signaling and causes mesenchymal transition of the coelomic epithelial cells early in Müllerian duct regression. *Development* 133(12):2359–2369.
63. Ha TU, et al. (2000) Mullerian inhibiting substance inhibits ovarian cell growth through an Rb-independent mechanism. *J Biol Chem* 275(47):37101–37109.
64. Bakkum-Gamez JN, et al. (2008) Müllerian inhibiting substance type II receptor (MISIIR): A novel, tissue-specific target expressed by gynecologic cancers. *Gynecol Oncol* 108(1):141–148.
65. Masiakos PT, et al. (1999) Human ovarian cancer, cell lines, and primary ascites cells express the human Mullerian inhibiting substance (MIS) type II receptor, bind, and are responsive to MIS. *Clin Cancer Res* 5(11):3488–3499.
66. Bergh A, Nikula H, Damber JE, Clayton R, Huhtaniemi I (1985) Altered concentrations of gonadotrophin, prolactin and GnRH receptors, and endogenous steroids in the abdominal testes of adult unilaterally cryptorchid rats. *J Reprod Fertil* 74(1):279–286.
67. Huhtaniemi I (1995) Molecular aspects of the ontogeny of the pituitary-gonadal axis. *Reprod Fertil Dev* 7(5):1025–1035.
68. Wang PY, et al. (2005) Mullerian inhibiting substance acts as a motor neuron survival factor in vitro. *Proc Natl Acad Sci USA* 102(45):16421–16425.
69. Wang PY, et al. (2009) Müllerian inhibiting substance contributes to sex-linked biases in the brain and behavior. *Proc Natl Acad Sci USA* 106(17):7203–7208.
70. Wittmann W, McLennan IS (2011) The male bias in the number of Purkinje cells and the size of the murine cerebellum may require Müllerian inhibiting substance/anti-Müllerian hormone. *J Neuroendocrinol* 23(9):831–838.
71. Clarkson AN, et al. (2011) Müllerian inhibiting substance is anterogradely transported and does not attenuate avulsion-induced death of hypoglossal motor neurons. *Exp Neurol* 231(2):304–308.
72. Hirschhorn T, et al. (2015) Constitutive negative regulation in the processing of the anti-Müllerian hormone receptor II. *J Cell Sci* 128(7):1352–1364.
73. Greene MR, MacCallum P (2012) Molecular Cloning: A Laboratory Manual (Cold Spring Harbor Lab Press, Plainview, NY), 4th Ed.
74. Hudson PL, et al. (1990) An immunoassay to detect human müllerian inhibiting substance in males and females during normal development. *J Clin Endocrinol Metab* 70(1):16–22.
75. Wei W, et al. (2013) FGF18 as a prognostic and therapeutic biomarker in ovarian cancer. *J Clin Invest* 123(10):4435–4448.
76. Thériault BL, Portelance L, Mes-Masson AM, Nachtigal MW (2013) Establishment of primary cultures from ovarian tumor tissue and ascites fluid. *Methods Mol Biol* 1049: 323–336.
77. Latifi A, et al. (2012) Isolation and characterization of tumor cells from the ascites of ovarian cancer patients: Molecular phenotype of chemoresistant ovarian tumors. *PLoS One* 7(10):e46858.
78. Donahoe PK, Ito Y, Hendren WH, 3rd (1977) A graded organ culture assay for the detection of Mullerian inhibiting substance. *J Surg Res* 23(2):141–148.